This is the accepted manuscript made available via CHORUS. The article has been published as:

Short-range atomic ordering in nonequilibrium silicon-germanium-tin semiconductors

S. Mukherjee, N. Kodali, D. Isheim, S. Wirths, J. M. Hartmann, D. Buca, D. N. Seidman, and O. Moutanabbir

Phys. Rev. B **95**, 161402 — Published 10 April 2017

DOI: 10.1103/PhysRevB.95.161402

Short-Range Atomic Ordering in Non-Equilibrium Silicon-Germanium-Tin Semiconductors

S. Mukherjee[1], N. Kodali[1], D. Isheim[2], S. Wirths[3], J. M. Hartmann[4], D. Buca[3], D. N. Seidman[2], and O. Moutanabbir[1,*]

[1] *Department of Engineering Physics, École Polytechnique de Montréal, Montréal, C. P. 6079, Succ. Centre-Ville, Montréal, Québec H3C 3A7, Canada.*

[2] *Department of Materials Science and Engineering and Northwestern University Center for Atom-Probe Tomography, Northwestern University, Evanston, IL 60208-3108, USA.*

[3] *Peter Grünberg Institute 9 and JARA - FIT, Forschungszentrum Juelich, Juelich 52425, Germany.*

[4] *CEA, LETI, Minatec Campus, 17 rue des Martyrs, Grenoble 38054, France.*

The precise knowledge of the atomic order in monocrystalline alloys is fundamental to understand and predict their physical properties. With this perspective, we utilized laser-assisted atom probe tomography to investigate the three-dimensional distribution of atoms in non-equilibrium epitaxial

Sn-rich group IV SiGeSn ternary semiconductors. Different atom probe statistical analysis tools including frequency distribution analysis, partial radial distribution functions, and nearest neighbor analysis were employed in order to evaluate and compare the behavior of the three elements to their spatial distributions in an ideal solid solution. This atomistic-level analysis provided clear evidence of an unexpected repulsive interaction between Sn and Si leading to the deviation of Si atoms from the theoretical random distribution. This departure from an ideal solid solution is supported by first principles calculations and attributed to the tendency of the system to reduce its mixing enthalpy throughout the layer-by-layer growth process.

The assumption that the arrangement of atoms within the crystal lattice is perfectly random is a broadly used approximation to establish the physical properties of semiconductor alloys. This approximation allows one to estimate rather accurately certain thermodynamic as well as material parameters like the excess enthalpy of formation, Vegard-like lattice parameters, and band gaps that are smaller than the composition weighted average (optical bowing). However, it has been proposed that some ternary semiconductors can deviate from this assumed perfect solid solution. Indeed, both calculations and experiments suggested the presence of local atomic order in certain III-V alloys [1–8]. This phenomenon manifests itself when at least one of the elements forming the alloy preferentially occupies or avoids specific lattice sites. This induces short-range order in the lattice with an impact on the basic properties of the alloyed semiconductors [3–7].

The recent progress in developing Sn-rich group IV (SiGeSn) ternary semiconductors and their integration in a variety of low dimensional systems and devices have revived the interest in elucidating the atomistic-level properties of monocrystalline alloys [9–20]. Interestingly, unlike III-V semiconductors, achieving a direct bandgap in $\mathrm{Si_xGe_{1-x-y}Sn_y}$ requires a sizable incorporation of Sn ($> 10\ at.\%$), which is significantly higher than the equilibrium solubility (<1 at.%). Understanding the atomic structure of these metastable alloys is therefore imperative for implementing predictive models to describe their basic properties. With this perspective, we present a first study of the atomic order in $\mathrm{Si_xGe_{1-x-y}Sn_y}$ alloys (x and y in $0.04-0.19$ and $0.02-0.12$ range, respectively). We employed Atom Probe Tomography (APT) which allows atomistic level investigations [21–24] and statistical tools to analyze the three-dimensional (3-D) distributions of the three elements. This analysis unraveled an unexpected repulsive interaction between Sn and Si leading to a deviation of Si atoms from the theoretical random distribution.

The samples investigated in this work were grown using a metal cold-wall reduced pressure chemical vapor deposition (CVD) [10,25,26] using Si_2H_6, Ge_2H_6, and $SnCl_4$ as precursors and a relatively low growth temperature of 350 - 475°C resulting in a normal growth rate of $\sim 1\mathrm{nm/s}$. Further details of epitaxial growth of $\mathrm{Si_xGe_{1-x-y}Sn_y}$ layers are described in the Supplemental Material, Ref [27]. Fig.1(a) shows the STEM images of the layer with highest Sn content ($\mathrm{Si_{0.04}Ge_{0.84}Sn_{0.12}}$), confirming the pseudomorphic growth of the ternary layers without dislocations or extended defects. Fig.1(b) shows the corresponding 3-D APT reconstructed map. The details of APT analysis along with data sets recorded from different layers are given in the Supplemental Material [27]. For cluster analysis, iso-concentration surfaces were first defined at varying Sn and Si concentrations within the reconstructed maps. No evidence of any aggregates was found regardless of the content. The mass spectra of Si, Ge, and Sn, displaying all the isotopes and the evaporated charge states are shown in Fig.S2 of the Supplemental Material [27]. In order to investigate the short-range atomic distribution, we performed a series of statistical analyses, namely the frequency distribution (FD) analysis, the partial radial distribution function (p-RDF) analysis, and the nearest neighbor (NN) analysis within pre-defined regions in 3-D maps. The theoretical formalism of each method is outlined in the Supplemental Material [27]. Fig.2(a) displays the FD of Si, Ge, and Sn in $\mathrm{Si_{0.04}Ge_{0.84}Sn_{0.12}}$. The coefficient of determination (R^2) between the observed value (y_i) and the binomial distribution (f_i) was calculated from the residual sum of squares, $S_{res} = \sum_i (y_i - f_i)^2$ and total sum of squares, $S_{tot} = \sum_i (y_i - \bar{y})^2$ and the relation $R^2 = 1 - {}^{S_{res}}\!/_{S_{tot}}$ with $\bar{y} = {}^{1}\!/_{n} \sum_{i=1}^{n} y_i$. The figure shows the mean values of the experimental FD for Si, Ge, and Sn correspond to 4.0, 84.0 and 12.0 at.%, respectively. This agrees with the concentrations found in the proximity histogram in Fig.S1(a) of the Supplemental Material [27]. Additionally, it reveals that while Ge and Sn closely follows the binomial distribution (calculated R^2 for Ge and Sn are 0.9999 and 0.9978 respectively), Si shows a small disagreement with binomial distribution (calculated R^2 for Si is 0.9679). We eliminate statistical fluctuations as a possible reason for this observed deviation because the probed volume is large enough to have a significant number of Si atoms. In Fig.2(b), we show the p-RDF of Sn and Si in $\mathrm{Si_{0.04}Ge_{0.84}Sn_{0.12}}$ with respect to (wrt.) Sn, Ge, and Si. It is worthwhile to state that in all analyses carried out for different layers, Ge is always found to be random. Henceforth, we shall restrict our discussion mainly to the behavior of Si and Sn. Also noteworthy is the fact that p-RDF is meaningful only for $r \geq 0.5\ nm$. For $r < 0.5nm$, APT data analysis program does not find any atom and generates random values for p-RDF. The p-RDF's in all the plots for $r < 0.5nm$ has been shaded. The following facts are evident from Fig.2(b): Si shows a negative correlation wrt. Sn and a positive correlation wrt. Ge as well as itself; Sn has its p-RDF at unity wrt. Ge and Si while it shows signs of a positive correlation wrt. itself. The p-RDF of Sn and Si wrt. Sn in the top panel in Fig 2(b) show a puzzling behavior. First, Sn is seen to have a positive correlation with itself. However, the FD and the NN distribution (later in Fig.4) do not give any indication that Sn deviates from a perfect random distribution. Second, the p-RDF's do not converge to unity at large values of r, unlike that in the lower two panels in Fig 2(b). We think that this unexpected behavior might be due to minute long-range compositional variations of Sn across the reconstructed APT maps.

The observations in Fig.2 provide clear evidence that Si atoms are disrupted from a perfect random distribution. The negative correlation shown by Si wrt. Sn hints at the presence of a repulsive interaction between the two species. This phenomenon provides new insights into the growth kinetics of metastable alloys by chemical vapor deposition [25], where the growth conditions prevent Sn atoms from forming equilibrium aggregated phase, despite the fact that the growth of a complete monolayer takes place in $\sim 0.1\mathrm{s}$ which is a very slow process compared to the time scale of surface diffusion events. The data presented in Fig.2 suggest that the repulsive interaction between Si and Sn is resulting from these elements diffusing away from each other during the growth, justifying the negative correlation of Si wrt. Sn. Note, that the p-RDF's are plotted relative to each other and normalized to the bulk concentration of an element. The repulsive interaction should have a subtle effect on the distribution of Sn and Ge as well, but the p-RDF's of Sn and Ge when plotted wrt. Si do not reflect this behavior due to their higher concentrations wrt. Si. The Si atoms diffusing away from Sn can either hop to other Ge atoms or make enough a large number of hops to other Si atoms (which are scarce). Hence, we see a positive correlation of Si wrt. Ge and also wrt. itself. Since bulk diffusion is energetically less favorable than surface diffusion, it is reasonable to conclude that the observed departure for an ideal solid solution occurs during the layer-by-layer growth. It is important to note that this phenomenon is peculiar to Sn-rich ternary alloys since extended x-ray absorption fine structure (EXAFS) investigations indicated the atomic distribution in Sn-rich strained and relaxed GeSn binary alloys to be random [28], also asserting the fact that epitaxial strain is not responsible for the observation we made in Fig 2.

Interestingly, the analysis of ternary layers with lower Sn contents ($\leq$ 4 at.%) indicates that the aforementioned departure from a perfectly random alloy is either absent or too small to be detected. For instance, Fig.3(a) exhibits the FD for each element in $\mathrm{Si_{0.10}Ge_{0.875}Sn_{0.025}}$. Noteworthy is the overlap between the observed distribution and the binomial distribution (black lines) assuming a complete random alloy (R^2 was calculated for Si, Ge, and Sn to be 0.9989, 0.9999, and 0.9959, respectively). Fig.3(b) shows the measured Sn and Si p-RDF within a sphere of radius $10\,\text{nm}$. Here, the p-RDF of Sn wrt. Sn shows the telltale signature of statistical fluctuations owing to its small concentration of only $2.5\text{ at.}\%$. The p-RDF fluctuates around the mean value of unity with the magnitude of these fluctuations decreases with increasing r. Note that the volume of the shell considered during p-RDF analysis and consequently the number of atoms which lies inside the shell increases as a function of r^2. Finally, the p-RDF of Sn steadies down to the value of unity. The p-RDF of Si wrt. Si and Sn are qualitatively similar, none showing any noticeable deviation from 1. The p-RDF of Sn wrt. Si, Ge and Si wrt. Ge, shown in Fig.S3 of the Supplemental Material [27], confirm that at low Sn content, all atoms are randomly distributed within the alloy, reinforcing the results of the FD analysis.

Fig.4(a) displays the analysis of NN distribution $NN_{A-A} - k$, where ‘A’ is Si or Sn; k is 2 (2nd NN), 3 (3rd NN), and 5 (5th NN) for $\text{Si}_{0.04}\text{Ge}_{0.84}\text{Sn}_{0.12}$. Fig 4(b) shows the departure of the observed NN distribution from the theoretical value, $P_k(r, C)$. The $NN - 1, 4, 10$ distribution for Si and Sn and their corresponding departure from $P_k(r, C)$ in $\text{Si}_{0.04}\text{Ge}_{0.84}\text{Sn}_{0.12}$ is shown in Fig.S4 of the Supplemental Material [27]. Fig 4 and Fig S4 show that while NN_{Sn-Sn} follow the probability distribution closely, NN_{Si-Si} does not. A shoulder starts to develop at a lower value of r than the maxima of $P_k(r, C)$ in the observed NN_{Si-Si} distribution, which gets more prominent with increasing k. The rest of the measured NN_{Si-Si} distribution shows a minute right shift relative to $P_k(r, C)$. These observed departures are clear indications of a disruption in Si distribution creating local pockets where there are more Si wrt. a given Si atom. In these pockets, the Si concentration is slightly higher than the average bulk concentration making the average distance between the NN’s slightly smaller than what is expected theoretically. The minute right shift also indicates that the rest of the matrix is slightly depleted of Si making the NN distances slightly larger than that in a perfect random distribution. The shoulder is obviously absent in $NN_{Si-Si}-1$ (Fig.S4(a)) due to the fact that no atom can be located at a distance smaller than the first nearest neighbor distance. Also noteworthy is the fact that such features are absent in the NN distributions within the alloy with low Sn content of $2.5\,\text{at.}\%$ (see Fig. S5 of the Supplemental Material [27]). The deviation shown NN_{Sn-Sn} in Fig S5(b) is purely random in nature owing to its small concentration, in contrast with the deviation shown by NN_{Si-Si} in Fig 4(b) (a +ve deviation below the maxima of $P_k(r,C)$, a $-$ve deviation at the maxima of $P_k(r,C)$, followed by a small +ve deviation above the maxima of $P_k(r,C)$).It must however be remembered that the observed deviation of Si in Sn-rich alloys from a perfect random atomic distribution must not be confused with the formation of aggregates [29,30].

The revelation that Si atoms in monocrystalline Sn-rich ternary alloys deviate from the behavior in an ideal solid solution is indeed surprising. We attributed this disruption in Si distribution to a repulsive interaction between the Sn and Si atoms. In order to elucidate the energetics of this phenomenon, we performed detailed DFT calculations using the Quantum Espresso code (details are provided in the Supplemental Material [27]) on a 32 atom supercell. As shown in Fig. S7 of the Supplemental Material [27], we found that a Si-Sn bond is indeed energetically not favorable requiring an additional energy of $\sim +50-250\,\text{meV/unit cell}$ as compared to the most stable configurations ($\text{NN}-3$ and $\text{NN}-4$). A similar observation was made during a recent EXAFS study on SiGeSn ternary alloys [31]. These calculations support qualitatively the hypothesized repulsive interaction between Si and Sn atoms. Here, it is important to notice that the incorporation of a large radius Sn atom in Ge lattice would create a local distortion leading to more compressive Ge regions around Sn. This seems to affect the incorporation of Si, which has a smaller radius, and perhaps prefers to incorporate in available sites far from these compressive regions. What we must remember, however, is that the growth of a metastable alloy is a kinetically controlled non-equilibrium process. Owing to limited mobility, atoms after deposition on the surface are inhibited to reach the equilibrium state within the growth time-scale. The problem therefore reduces to a surface process where one needs to evaluate how atoms behave at the surface before they become buried underneath the next growing layer. Herein, one can reasonably neglect bulk diffusion as it implies energy barriers that are significantly higher than those for surface diffusion. One can also intuitively assume that, once atoms are deposited on a surface, the system will begin to evolve to minimize the mixing enthalpy ΔH_{mix} in an effort to reduce its Gibbs free energy. This evolution is abruptly brought to an end after the next growing layer sweeps across the entire surface. Since Ge is the solvent and Si and Sn are solutes, the mixing

enthalpy ΔH_{mix} is given by: $\Delta H_{mix} = H_{alloy} - xH_{Si} - (1-x-y)H_{Ge} - yH_{Sn}$. With the mole fractions and the enthalpies of the pure elements (H_{Si}, H_{Ge}, H_{Sn}) predetermined, H_{alloy} becomes a determining parameter. H_{alloy} is affected by factors like epitaxial strain, micro-strain, and chemical interaction. Micro-strain arises when the lattice has to accommodate two atoms of dissimilar size yet maintaining a uniform lattice constant throughout the crystal. For example, with

N the total number of atoms and $\Omega_{\mathrm{Si-Sn}}$ the Si-Sn interaction parameter, the micro-strain contribution coming from Si-Sn bonds in a regular solution is given by $N\Omega_{Si-Sn}(xy)$. Unlike the epitaxial strain and micro-strain whose contribution to H_{alloy} is always positive, the chemical interaction contribution (ΔH_{Ch}) to H_{alloy} can be positive or negative. This depends on the nature of charge transfer between two atoms forming a bond. For example, calculations showed that in ordered $\mathrm{GaInP_2}$ the difference in electronegativity between the atoms caused charge to flow from the less ionic $\mathrm{Ga-P}$ bond to the more ionic $\mathrm{In-P}$, giving a small positive value of ΔH_{Ch} [1]. The process of charge transfer takes place not only for bonding atoms which belong to different groups (hence different electronegativity) but also for isovalent heteropolar atoms like group IV elements. Indeed, first-principle calculations found a small positive and a small negative value of ΔH_{Ch} for SiGe and SiC respectively [32].

In summary, we performed atomic scale studies on Sn-rich metastable SiGeSn ternary alloys using APT. To investigate the randomness in the distribution of different atoms within the alloys, we implemented different statistical techniques, namely the FD, p-RDF's, and the NN distribution. Our study shows that the Si atoms deviate from a perfectly random solid solution within the alloy with large Sn content. The phenomenon is attributed to a repulsive interaction between Sn and Si, thereby inducing local disruptions in an otherwise random distribution of Si. The DFT calculations also demonstrated that having Si and Sn atoms as nearest neighbors is indeed energetically unfavorable. These departures from an ideal solid solution shown by Si is either absent or too weak to be detected in alloys with low Sn content ($< 4\ at.\%$). The observed short range ordering must be taken into account for a more accurate evaluation of lattice parameter, lattice relaxation, thermodynamic parameters, band structure, and opto-electronic properties of group IV ternary semiconductors.

Acknowledgment. The work was supported by NSERC-Canada, Canada Research Chair, Calcul Québec, and Compute Canada. The LEAP at the Northwestern University Center for Atom-Probe Tomography (NUCAPT) was acquired and upgraded with equipment grants from the MRI program of the National Science Foundation (grant number DMR-0420532) and the DURIP program of the Office of Naval Research (grant numbers N00014-0400798, N00014-0610539, N00014-0910781). NUCAPT is supported by the NSF's MRSEC program (grant number DMR-1121262). Additional instrumentation at NUCAPT was supported by the Initiative for Sustainability and Energy at Northwestern (ISEN).

---

*Corresponding author.
oussama.moutanabbir@polymtl.ca

Reference

[1] G. P. Srivastava, J. L. Martins, and A. Zunger, Phys. Rev. B **31**, 2561 (1985).

[2] M. Ichimura and A. Sasaki, J. Appl. Phys. **60**, 3850 (1986).

[3] A. Mascarenhas, S. Kurtz, A. Kibbler, and J. Olson, Phys. Rev. Lett. **63**, 2108 (1989).

[4] T. Kanata, M. Nishimoto, H. Nakayama, and T. Nishino, Phys. Rev. B **45**, 6637 (1992).

[5] D. C. Meyer, K. Richter, P. Paufler, and G. Wagner, Phys. Rev. B **59**, 15253 (1999).

[6] L. Alagna, T. Prosperi, S. Turchini, C. Ferrari, L. Francesio, and P. Franzosi, J. Appl. Phys. **83**, 3552 (1998).

[7] C. Bocchi, P. Franzosi, and C. Ghezzi, J. Appl. Phys. **57**, 4533 (1985).

[8] T. Kuan, T. Kuech, W. Wang, and E. Wilkie, Phys. Rev. Lett. **54**, 201 (1985).

[9] A. Attiaoui and O. Moutanabbir, J. Appl. Phys. **116**, 63712 (2014).

[10] S. Wirths, A. T. Tiedemann, Z. Ikonic, P. Harrison, B. Holländer, T. Stoica, G. Mussler, M. Myronov, J. M. Hartmann, D. Grützmacher, D. Buca, and S. Mantl, Appl. Phys. Lett. **102**, 192103 (2013).

[11] G. Sun, H. H. Cheng, J. Menéndez, J. B. Khurgin, and R. A. Soref, Appl. Phys. Lett. **90**, 251105 (2007).

[12] J. D. Gallagher, C. Xu, L. Jiang, J. Kouvetakis, and J. Menéndez, Appl. Phys. Lett. **103**, 202104 (2013).

[13] J. Kouvetakis, J. Menendez, and A. V. G. Chizmeshya, Annu. Rev. Mater. Res. **36**, 497 (2006).

[14] P. Moontragoon, R. A. Soref, and Z. Ikonic, J. Appl. Phys. **112**, 73106 (2012).

[15] K. Lu Low, Y. Yang, G. Han, W. Fan, and Y.-C. Yeo, J. Appl. Phys. **112**, 103715 (2012).

[16] S. Gupta, B. Magyari-Ko□pe, Y. Nishi, and K. C. Saraswat, J. Appl. Phys. **113**, 73707 (2013).

[17] R. Kotlyar, U. E. Avci, S. Cea, R. Rios, T. D. Linton, K. J. Kuhn, and I. A. Young, Appl. Phys. Lett. **102**, 113106 (2013).

[18] M. Oehme, D. Widmann, K. Kostecki, P. Zaumseil, B. Schwartz, M. Gollhofer, R. Koerner, S. Bechler, M. Kittler, E. Kasper, and J. Schulze, Opt. Lett. **39**, 4711 (2014).

[19] S. Takeuchi, A. Sakai, K. Yamamoto, O. Nakatsuka, M. Ogawa, and S. Zaima, Semicond. Sci. Technol. **22**, S231 (2007).

[20] R. Chen, S. Gupta, Y.-C. Huang, Y. Huo, C. W. Rudy, E. Sanchez, Y. Kim, T. I. Kamins, K. C. Saraswat, and J. S. Harris, Nano Lett. **14**, 37 (2014).

[21] S. Mukherjee, H. Watanabe, D. Isheim, D. N. Seidman, and O. Moutanabbir, Nano Lett. **16**, 1335 (2016).

[22] E. P. Silaeva, L. Arnoldi, M. L. Karahka, B. Deconihout, A. Menand, H. J. Kreuzer, and A. Vella, Nano Lett. **14**, 6066 (2014).

[23] D. E. Perea, I. Arslan, J. Liu, Z. Ristanović, L. Kovarik, B. W. Arey, J. A. Lercher, S. R. Bare, and B. M. Weckhuysen, Nat. Commun. **6**, 7589 (2015).

[24] W. Chen, L. Yu, S. Misra, Z. Fan, P. Pareige, G. Patriarche, S. Bouchoule, and P. R. I. Cabarrocas, Nat. Commun. **5**, 4134 (2014).

[25] J.-H. Fournier-Lupien, S. Mukherjee, S. Wirths, E. Pippel, N. Hayazawa, G. Mussler, J. M. Hartmann, P. Desjardins, D. Buca, and O. Moutanabbir, Appl. Phys. Lett. **103**, 263103 (2013).

[26] S. Wirths, D. Buca, and S. Mantl, Prog. Cryst. Growth Charact. Mater. **62**, 1 (2016).

[27] See Supplemental Material at (link) for details of epitaxial gowth of the alloys and the atom probe investigation; the theoretical background of the statistical tools; additional results concenring the statistical analysis on the atom prbe data set; and the DFT calculations.

[28] F. Gencarelli, D. Grandjean, Y. Shimura, B. Vincent, D. Banerjee, A. Vantomme, W. Vandervorst, R. Loo, M. Heyns, and K. Temst, J. Appl. Phys. **117**, 95702 (2015).

[29] R. K. W. Marceau, L. T. Stephenson, C. R. Hutchinson, and S. P. Ringer, Ultramicroscopy **111**, 738 (2011).

[30] F. De Geuser, W. Lefebvre, and D. Blavette, Philos. Mag. Lett. **86**, 227 (2006).

[31] Y. Shimura, T. Asano, T. Yamaha, M. Fukuda, W. Takeuchi, O. Nakatsuka, and S. Zaima, Mater. Sci. Semicond. Process. (2016).

[32] J. Martins and A. Zunger, Phys. Rev. Lett. **56**, 1400 (1986).

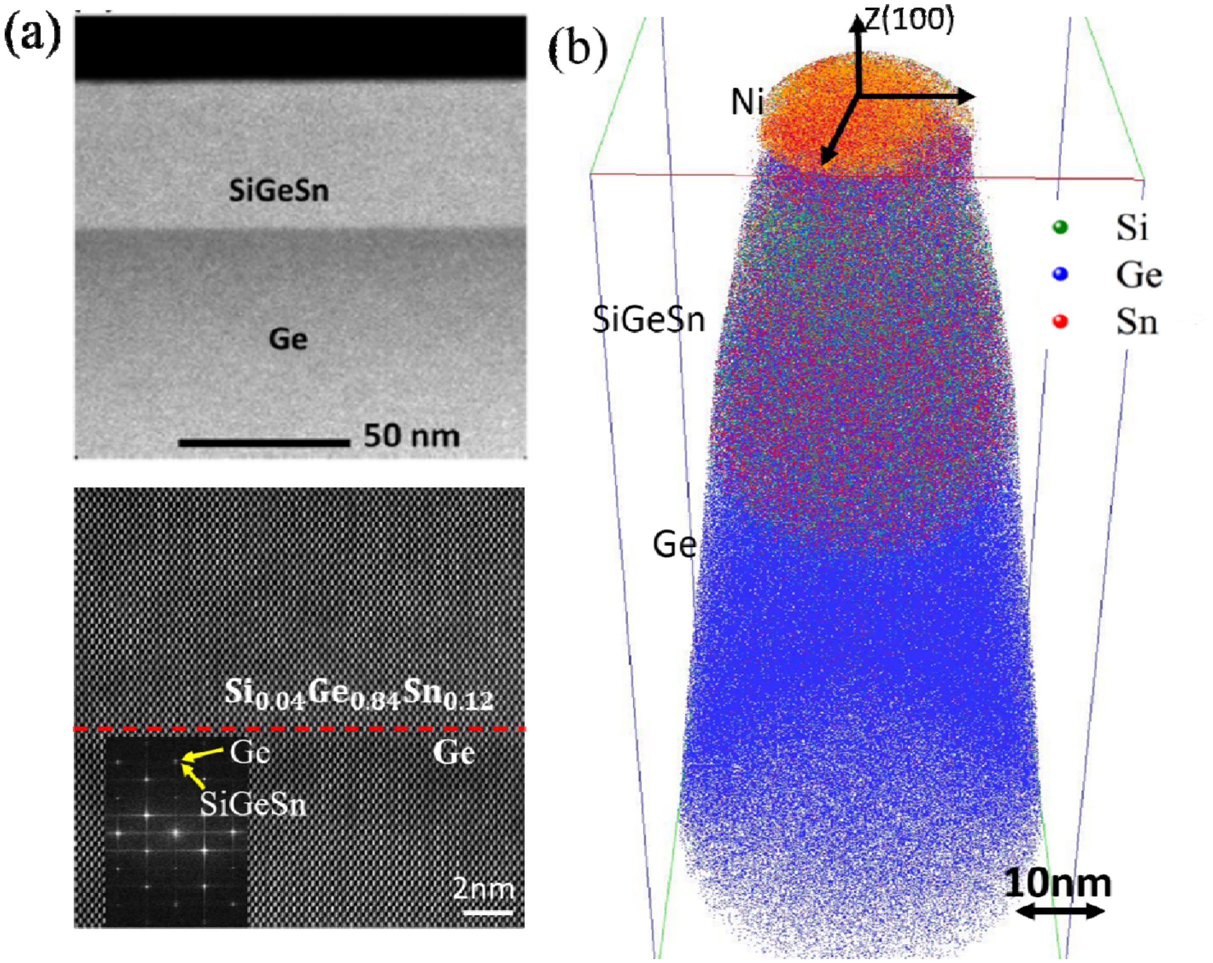
(a)
SiGeSn
Ge
50 nm
$Si_{0.04}Ge_{0.84}Sn_{0.12}$
Ge
SiGeSn
Ge
2nm
(b)
Z(100)
Ni
SiGeSn
Ge
Si
Ge
Sn
10nm

FIG. 1. (a) High angle annular dark field STEM (top) and high resolution STEM (bottom) images of the /Ge interface. Inset: A diffraction pattern taken from a selected region at the interface (b) 3-D reconstruction of the ternary alloy , showing the Ni capping layer, the SiGeSn thin film and a portion of the Ge buffer layer. For the sake of clarity, only 10% of Ge atoms and 50% of Sn atoms are displayed

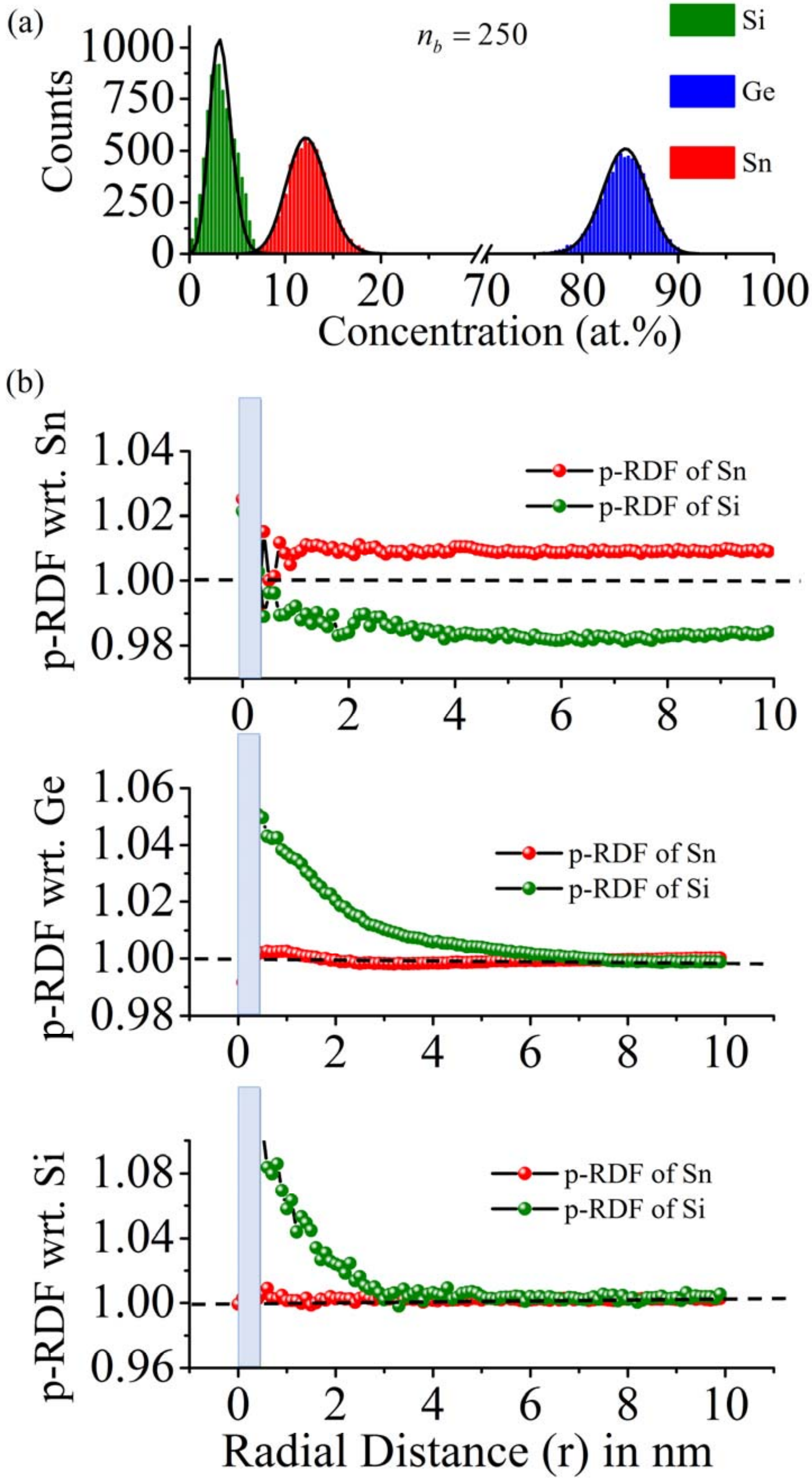
(a)
$n_b = 250$
Si
Ge
Sn
Counts
1000
750
500
250
0
0
10
20
70
80
90
100
Concentration (at.%)
(b)
p-RDF wrt. Sn
1.04
1.02
1.00
0.98
p-RDF of Sn
p-RDF of Si
0
2
4
6
8
10
p-RDF wrt. Ge
1.06
1.04
1.02
1.00
0.98
p-RDF of Sn
p-RDF of Si
0
2
4
6
8
10
p-RDF wrt. Si
1.08
1.04
1.00
0.96
p-RDF of Sn
p-RDF of Si
0
2
4
6
8
10
Radial Distance (r) in nm

FIG. 2. (a) Frequency distribution of Si (green), Ge (blue), and Sn (red) in $\mathrm{Si_{0.04}Ge_{0.84}Sn_{0.12}}$ as determined from APT reconstruction (in histograms). The corresponding binomial distribution of these atoms are shown in black continuous lines (b) The partial radial distribution function of Sn and Si atoms with respect to Sn (top), Ge (middle), and Si (bottom) in the same sample as in (a) for $\mathrm{r = 10nm}$. The IVAS computed error bars are smaller than the data symbols. The black dotted line represents $\mathrm{p - RDF\ = 1}$

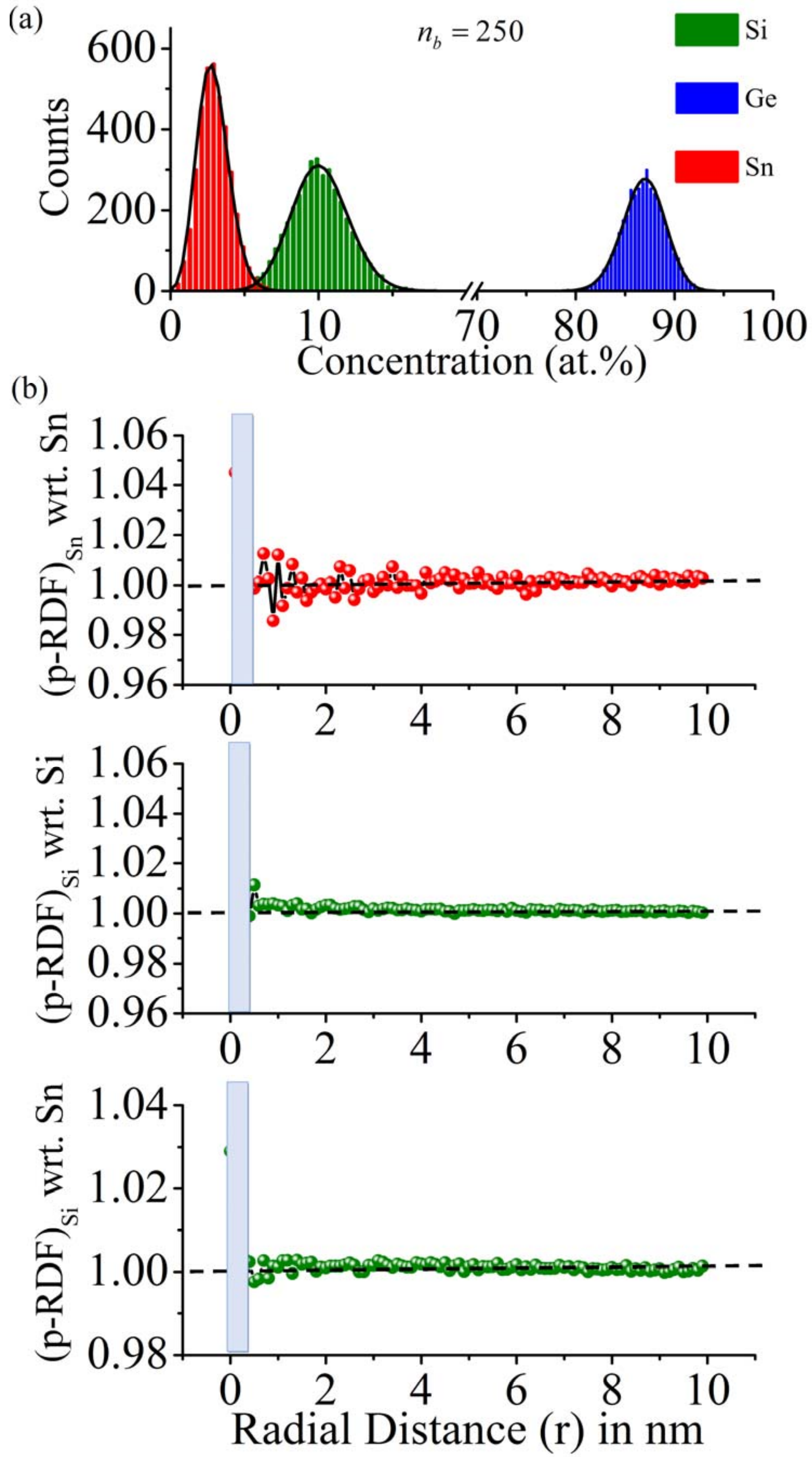
(a)
$n_b = 250$
Si
Ge
Sn
Counts
0
200
400
600
0
10
70
80
90
100
Concentration (at.%)
(b)
(p-RDF)$_{Sn}$ wrt. Sn
1.06
1.04
1.02
1.00
0.98
0.96
0
2
4
6
8
10
(p-RDF)$_{Si}$ wrt. Si
1.06
1.04
1.02
1.00
0.98
0.96
0
2
4
6
8
10
(p-RDF)$_{Si}$ wrt. Sn
1.04
1.02
1.00
0.98
0
2
4
6
8
10
Radial Distance (r) in nm

FIG. 3. (a) Frequency distribution of Si (green), Ge (blue), and Sn (red) in $\mathrm{Si_{0.10}Ge_{0.875}Sn_{0.025}}$ as determined from APT reconstruction (in histograms). The corresponding binomial distribution of these atoms are shown in black continuous lines. (b) The partial radial distribution function in the same sample as (a) for $\mathrm{r = 10nm}$ of Sn atoms wrt. Sn (top), Si wrt. Si (middle), and Si wrt. Sn (bottom). The IVAS computed error bars are smaller than the data symbols. The black dotted line represents $\mathrm{p - RDF = 1}$

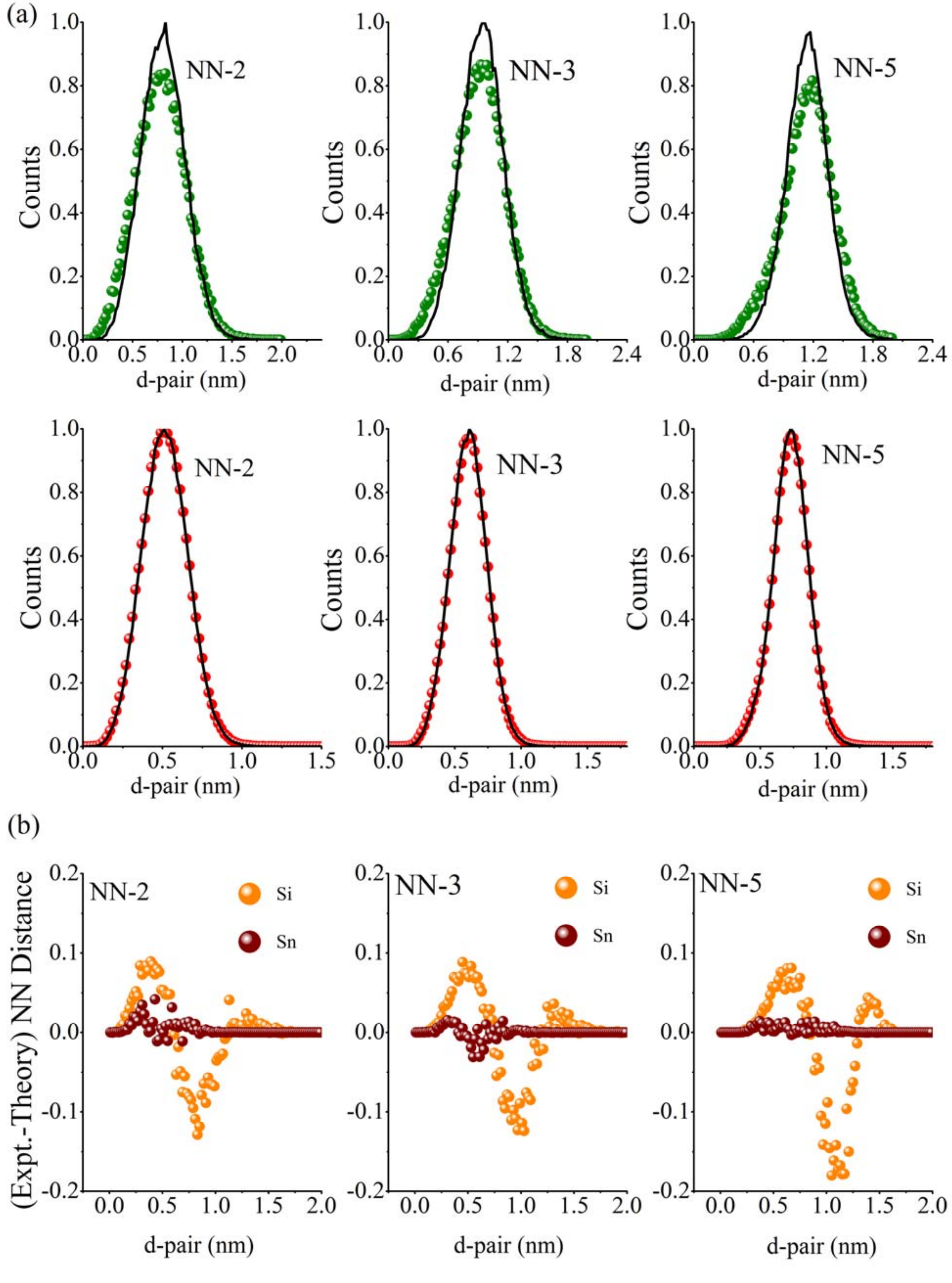
(a)
NN-2
NN-3
NN-5
Counts
d-pair (nm)
0.0
0.2
0.4
0.6
0.8
1.0
0.5
1.5
2.0
0.6
1.2
1.8
2.4
(b)
(Expt.-Theory) NN Distance
Si
Sn
-0.2
-0.1
0.1
0.2

FIG. 4. (a) Si-Si and Sn-Sn NN 2, 3, and 5 distribution in the alloy containing 12.0 at.% Sn. The distribution as determined from APT reconstruction are shown in solid spheres Si (green) and Sn (red). The corresponding binomial distribution are shown in black continuous lines. All the data sets are normalized with respect to the theoretical probability distribution, $P_k(r, C)$.(b) Departure of the observed Si-Si and Sn-Sn NN 2, 3, and 5 distributions from the binomial distribution. The y-axis in all the three figures are the same.